A Volume-Surface Integral Equation Method for Solving Maxwell's Equations in Electrically Inhomogeneous Media Using Tetrahedral Grids

Jacek Nadobny, Peter Wust, Martin Seebass, Peter Deuflhard, and Roland Felix

Abstract— **Starting with the solution of Maxwell's equations based on the volume integral equation (VIE) method, the transition to a volume-surface integral equation (VSIE) formulation is described. For the VSIE method, a generalized calculation method is developed to help us directly determine E fields at any interface combination in three-dimensional (3-D) electrically inhomogeneous media. The VSIE implementation described here is based on separating the domain of interest into discrete parts using nonuniform tetrahedral grids. Interfaces are described using curved or plane triangles. Applying linear nodal elements, a general 3-D formulation is developed for handling scatter field contributions in the immediate vicinity of grid nodes, and this formulation is applicable to all multiregion junctions. The special case of a smooth interface around a grid node is given naturally by this formulation. Grid nodes are split into pairs of points for E-field calculation, and node normals are assigned to these points. The pairs of points are assigned to the elements adjoining the grid node. For each pair of points, the correct field jumps on the interface are given by a surface integral over the polarization surface charge density.**

Discretization Nomenclature

As a guide to the reader we have summarized the symbols and definitions used below.

Q	Grid point/grid node: point, where N surface elements $\Gamma^{(i)}$ $(i = 1, \cdots, N)$ meet and subdivide 2 or more subregions $\epsilon_1, \epsilon_2, \cdots$ (Figs. 4 and 5).
$\Gamma^{(i)}$	Gurved triangular surface element i (Figs. 3 and 4).
$\Lambda^{(i)}$	Plane triangular surface grid element i approximating $\Gamma^{(i)}$ (Figs. 3 and 6).
$\boldsymbol{n}^{(i)}$	Unit nodal normal on $\Gamma^{(i)}$ "at" Q (separation from Q infinitesimal) defined in (14) (Figs. 3 and 4).
$\Psi^{(i)}$	Projection of $\Gamma^{(i)}/\Lambda^{(i)}$ on the tangential plane $\perp \boldsymbol{n}^{(i)}$ (Figs. 6 and 7).
$V_\delta(Q)$	Spherical neighborhood surrounding Q with radius δ (Figs. 4 and 5).
$\Gamma_\delta^{(i)}\ V_\delta(Q) \cap \Gamma^{(i)}$	(Figs. 3–5).
$\Gamma_{>\delta}^{(i)}\ \Gamma^{(i)} \backslash \Gamma_\delta^{(i)}$	(Fig. 5).
$P^{(i)}$	Reference point generated by splitting off the grid node Q, associated with $\Gamma_\delta^{(i)}$ (Fig. 5).
$P_{+/-}^{(i)}$	Pair of reference points for E-field calculation generated by splitting off $P^{(i)}$ (Fig. 5).
$\Rightarrow$	Used to indicate the integral contribution of Γ or Ψ to $P_{+/-}$.

Manuscript received April 10, 1995; revised December 18, 1995. This work was supported in part by Berliner Sparkassenstiftung Medizin, Deutsche Krebshilfe e.V. (Grant M7/94Fe9), and by Deutsche Forschungsgemeinschaft (SFB 273).

J. Nadobny, P. Wust, and R. Felix are with Strahlenklinik und Poliklinik, Virchow Klinikum–Humboldt Universitaet zu Berlin, 13344 Berlin, Germany.

M. Seebass, P. Deuflhard, and J. Nadobny are with Konrad-Zuse-Zentrum fuer Informationstechnik Berlin (ZIB), 10711 Berlin, Germany.

Publisher Item Identifier S 0018-9480(96)02333-2.

I. Introduction

THE recent fast-paced development of computer technology now enables the calculation of electromagnetic fields in complicated three-dimensional (3-D) models. One important application area for these field calculations is, e.g., hyperthermia. In order to determine the temperature in a patient's body we need to know the distribution of the absorbed power density, and in biological media this is proportional to the conductivity of the tissue and the square of the contribution made by the electric field strength. Electrical properties of neighboring tissue compartments meeting at interfaces can contrast very strongly (e.g., bone/muscle interface and fat/muscle interface). This means that to perform these model calculations accurately enough we must take precise account of local interface details such as curvature, torsion, etc. Nonsmooth interfaces like corners and wedges, and points at which three or more electrically different media meet and where no clear interface standard is definable, so-called multiregion points, must also be included in our numerical considerations.

The singular behavior of E-fields near nonsmooth interfaces (in 2-D TE cases) has already been theoretically described in [1] and [2]. A similar singular field behavior can be observed in biological media at multiregion points. These points are a serious obstacle to numerical hyperthermia-modeling methods, regardless of whether the integration technique used is local (finite elements method (FEM), finite-difference time-domain (FDTD) method, or finite integration technique (FIT) method) or global (boundary elements method (BEM), or integral equation (IE) methods). In [3] and [4], elements with special E-field interpolations were applied to 2-D TE cases in order to reconstruct the singular field behavior described in [1] and [2]. As far as the authors are aware, a generalization relating to the 3-D case has not yet been constructed. An appropriate way to deal with these singularities may be the use

of edge elements or combined node/edge elements for the FEM [5]–[6] in combination with local refinement on tetrahedral grids; however, these techniques have until now only been applied to comparatively simple 3-D structures. For realistic patient modeling, a finite elements (FE) method was described recently [7] in which the E-field values in critical regions can be determined indirectly from the calculated potentials or H-field distribution. This method uses tetrahedral nodal elements. In the conjugate gradient fast Fourier transformation (CGFFT) method [8] which solves the volume integral equation (VIE) on uniform cubic grids, the E-field distribution is also determined indirectly from the calculated potentials. The recently presented global multiple multipole (MMP) method [9] achieves a good accuracy, in particular near boundaries, but it shows strong practical limitations for scatterers with complicated angular shapes or inhomogeneous bodies. Finite differences (FD) and finite integration (FI) techniques for calculating 3-D field distributions in inhomogeneous media—such as the FDTD method [10]–[15], and the FIT method [16]–[17]—can be applied to strongly heterogeneous structures, but they require uniform cubic grids and show difficulties in modeling curved or sloped interfaces. As far as the authors know, no algorithm for nodal elements has yet been described whose construction takes explicitly into account E-field behavior at arbitrary 3-D interface combinations. This applies especially to locations at which a singular E-field behavior is expected.

In [18] we introduced a basis version of an algorithm for the VSIE method for linear nodal tetrahedral elements with which explicit E-field modeling has already been performed on combinations of interface wedges, corners, and multiregion points. We described there the numerical procedure for forcing the boundary conditions at interfaces by defining a suitable polarization surface charge density η at the pair of points for E-field calculation (linking with the normal flux density D_n), and forming the limes ("self-contribution") of the strongly singular integral over η. In [18] we also performed a code comparison between the VSIE method and the FIT method [16]–[17], testing various iterative methods for solving the linear system of equations given by the VSIE method. The most effective solver for VSIE proved to be GMRES [19].

While in [18] the treatment of 3-D structures with nonsmooth interfaces was limited to the special case of an inhomogeneous cylinder, in this paper an improved general VSIE calculation method is developed using linear nodal elements for arbitrary 3-D combinations of electrical interfaces, including smooth structures, and structures with corners and/or edges. In contrast to [18], the "special case" of a smooth interface around a grid node is given naturally and consistently by this formulation. In order to achieve sufficient accuracy when determining the E-field in the immediate proximity of interface elements, the integration is analytically performed over these elements. During this integration, local characteristics of the interface are taken into account using special numerical procedures such as describing E-fields as their tangential and perpendicular components and splitting grid nodes. In order to avoid overestimating the influence of field singularities at nonsmooth interfaces, an optimal grid-dependent omission radius is estimated for linear interpolations using local polarization charge shifts (see Appendix). The plausibility of the estimate is confirmed using suitable numerical energy studies of a layered cube. Further numerical VSIE results for different geometries can also be found in [20].

II. Numerical Method

A. Description of the VSIE Method

1) General Volume Formulation (VIE): For an inhomogeneous domain of interest, which is embedded in an unbounded homogeneous background medium ϵ_b, Maxwell's Equations can be formulated in terms of the known incident field and the unknown scattered field

$$\boldsymbol{E} = \boldsymbol{E}_{\text{inc}} + \boldsymbol{E}_{\text{scat}} \tag{1a}$$

$$\boldsymbol{H} = \boldsymbol{H}_{\text{inc}} + \boldsymbol{H}_{\text{scat}}. \tag{1b}$$

The incident fields $\boldsymbol{E}_{\text{inc}}$, $\boldsymbol{H}_{\text{inc}}$ are defined as electromagnetic fields remaining if the domain of interest is replaced by the background medium ϵ_b. Conceptual basis of the integral equation (IE) formulation is the substitution of the electrical heterogeneities by apparent (or polarization) electric and magnetic sources radiating into the unbounded background medium (Fig. 1). These apparent sources generate the scattered fields $\boldsymbol{E}_{\text{scat}}$, $\boldsymbol{H}_{\text{scat}}$—and the Green's function of the background medium ϵ_b describes their radiation behavior.

We begin with the assumption that within the domain of interest V, the electromagnetic material properties ϵ and μ and the fields H and E can all be represented as continuous local functions (V includes the inhomogeneous boundary layer between the domain of interest and the background medium). This allows us to start by giving IE (1a) and (1b) as a general volume formula without a surface integral (see Problem I in [21, p. 285]). Cases with discontinuous material properties can then be processed using suitable interface integrals that can be derived from the general volume formula [see (10)].

In particular, if a magnetically homogeneous domain is assumed (constant permeability $\mu = \mu_0$ in biological media!) the integral equation for $\boldsymbol{E}$ ((1a), see [21, p. 287]) becomes

$$\begin{aligned}\boldsymbol{E}_{\text{scat}} &= -j\omega\mu_0 \int_V \boldsymbol{J}(\boldsymbol{r}')g(\boldsymbol{r}, \boldsymbol{r}')\, d^3r' \\ &\quad + \frac{1}{\epsilon_b}\int_V \rho(\boldsymbol{r}')\vec{\nabla}' g(\boldsymbol{r}, \boldsymbol{r}')\, d^3r' \\ &= \boldsymbol{T}_1(\boldsymbol{E}) + \boldsymbol{T}_2(\boldsymbol{E})\end{aligned} \tag{2}$$

where apparent volume current density

$$\boldsymbol{J}(\boldsymbol{r}') = j\omega(\epsilon(\boldsymbol{r}') - \epsilon_b)\boldsymbol{E}(\boldsymbol{r}') \tag{3}$$

apparent volume charge density

$$\rho(\boldsymbol{r}') = \frac{-\epsilon_b}{\epsilon(\boldsymbol{r}')}(\boldsymbol{E}(\boldsymbol{r}')\vec{\nabla}'\epsilon(\boldsymbol{r}')) \tag{4}$$

scalar Green's Function of the background medium

$$g(\boldsymbol{r}, \boldsymbol{r}') = \frac{1}{4\pi|\boldsymbol{r} - \boldsymbol{r}'|}e^{-jk|r-r'|} \tag{5}$$

the gradient of the scalar Green's function

$$\vec{\nabla}' g(\boldsymbol{r}, \boldsymbol{r}') = \frac{\boldsymbol{r} - \boldsymbol{r}'}{4\pi|\boldsymbol{r} - \boldsymbol{r}'|^3} \cdot (jk|\boldsymbol{r} - \boldsymbol{r}'| + 1) \cdot e^{-jk|r-r'|} \quad (6)$$

propagation constant of the background medium

$$k = \omega\sqrt{\mu_0 \epsilon_b}. \quad (7)$$

A harmonic time dependence ($e^{j\omega t}$) is assumed. $\boldsymbol{E}$, $\boldsymbol{J}$, ρ, ϵ are complex quantities ($\epsilon = \epsilon_0 \epsilon^{rel} - j\sigma/\omega$ in biological media). In contrast to the weakly singular integral $\boldsymbol{T}_1(\boldsymbol{E})$, the strongly singular integral $\boldsymbol{T}_2(\boldsymbol{E})$ does not disappear in (2) for $\boldsymbol{r} \to \boldsymbol{r}'$ (see (19) in Section III-C).

2) Transition to a Volume-Surface Formulation (VSIE): Many electromagnetic problems lead to the domain of interest being split up into electrically homogeneous subdomains ϵ_i as shown in Fig. 1. For this type of problems, the value of grad (ϵ) in (4) is other than zero only inside the thin inhomogeneous boundary layers between the homogeneous subdomains and between the subdomains and the background medium. Thus, the volume integral $\boldsymbol{T}_2(\boldsymbol{E})$ over thin boundary layers can be transformed into a surface integral over interfaces. This change is illustrated for a boundary layer ϵ_1/ϵ_2 of thickness τ (see Fig. 2). The layer is discretized using differential cubic volume elements of side length κ ($i = 1, \cdots, N_I$, $N_1 = \tau/\kappa$, $j = 1, \cdots, N_J$, $N_J \gg N_I$). In index direction i, i.e., perpendicular to the boundary layer, a linear (and therefore continuous) transition from ϵ_1 to ϵ_2 is assumed. In volume element (i, j), the discretization of (4) gives

$$\rho(i, j) = -\epsilon_b \frac{1}{\kappa} \cdot \frac{\epsilon(i+1) - \epsilon(i)}{\epsilon(i) + \epsilon(i+1)} (E_n(i) + E_n(i+1)). \quad (8)$$

In this equation, only the E-field component perpendicular to the boundary layer, i.e., in direction grad (ϵ) contributes to the result. Introducing the interface condition for electrical flux density $\epsilon(i)E_n(i) = D_n$ for all $i = 1, \cdots, \tau/\kappa$, we get

$$\rho(i, j) = \epsilon_b \frac{1}{\kappa} \cdot \left(\frac{1}{\epsilon(i+1)} - \frac{1}{\epsilon(i)} \right) D_n. \quad (9)$$

As τ tends towards zero, the boundary layer becomes an interface Γ and $\boldsymbol{T}_2(\boldsymbol{E})$ becomes a surface integral over Γ

$$\lim_{\tau \to 0} \boldsymbol{T}_2(\boldsymbol{E}) = \overline{\boldsymbol{T}}_2(\boldsymbol{E}) = \frac{1}{\epsilon_b} \int_\Gamma \eta(\boldsymbol{r}') \vec{\nabla} g(\boldsymbol{r}, \boldsymbol{r}')\, d^2 r' \quad (10)$$

where (complex) apparent surface charge density is given by

$$\eta = \epsilon_b \left(\frac{1}{\epsilon_2} - \frac{1}{\epsilon_1} \right) D_n = \epsilon_b \frac{\epsilon_1 - \epsilon_2}{\epsilon_1 \cdot \epsilon_2} D_n. \quad (11)$$

Finally, with (10), (1a) and (2) can be formulated as the so called volume-surface integral equation (VSIE)

$$\boldsymbol{E} = \boldsymbol{T}_1(\boldsymbol{E}) + \overline{\boldsymbol{T}}_2(\boldsymbol{E}) + \boldsymbol{E}_{\text{inc}}. \quad (12)$$

This formulation was used as a basis by Wust *et al.* in [18].

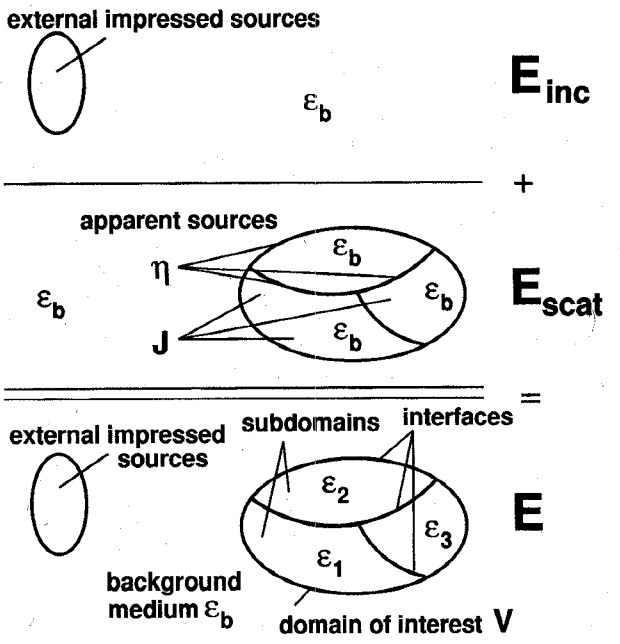

Fig. 1. Induced polarization and homogenization principle for VSIE. The domain of interest V consists of sections of homogeneous subdomains ϵ_i and is surrounded by a homogeneous unbounded background medium ϵ_b. In the domain of interest, ϵ_i can be replaced by ϵ_b if suitable apparent (polarization) sources are defined; apparent volume current density $\boldsymbol{J}$ in V, apparent surface charge density η on the internal interfaces between the subdomains ϵ_i and on the outer interface between V and the background medium. The entire field problem can be solved using a single Green's function for the background medium (homogenization). The total field $\boldsymbol{E}$ is the sum of the known incident field $\boldsymbol{E}_{\text{inc}}$ and the unknown scattered field $\boldsymbol{E}_{\text{scat}}$ (generated by apparent sources) which is linearly dependent on $\boldsymbol{E}$. In this formulation, the incident fields are generated by external impressed sources, but a coupling between sources and the domain of interest can generally also be taken into account (not shown here).

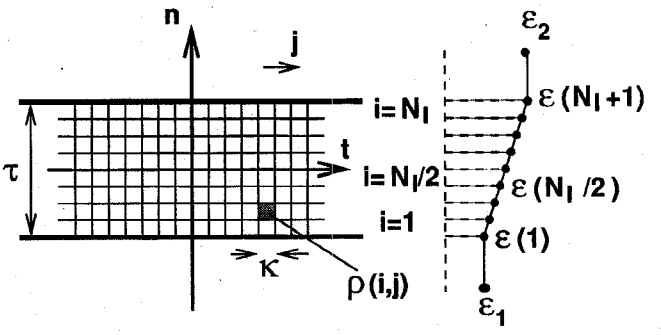

Fig. 2. Transition from volume (VIE) to surface (VSIE) formulation for a boundary layer. A boundary layer of thickness τ which lies between two homogeneous subdomains ϵ_1 and ϵ_2 is discretized using differential cubic volume elements (i, j) of side length κ. In the index direction $i = 1, \cdots, \tau/\kappa$, i.e., perpendicular to the boundary layer, a linear (therefore continuous) transition is assumed between ϵ_1 and ϵ_2. For $\tau \to 0$, the layer turns into an interface Γ and the strongly singular volume integral over the apparent volume charge density becomes a surface integral over the apparent surface charge density.

B. Discretization Procedure of the VSIE

1) Linear Equation System: The VSIE method can be applied to any kind of volume or interface elements. However, to discretize random irregular structures with curved interfaces (such as tissue compartments in biological media), tetrahedral grids [22] are the suitable type of grid.

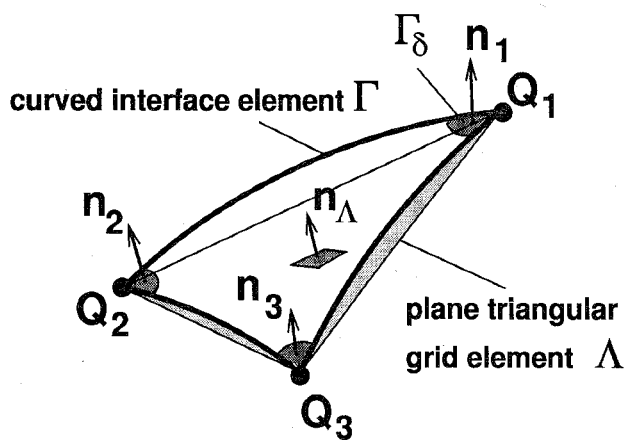

Fig. 3. Discretization of interfaces of arbitrary curved geometries. A curved triangular element Γ is given by grid nodes Q_j $(j = 1, \cdots, 3)$. For every grid node Q_j a nodal normal $\boldsymbol{n}_j$ with respect to Γ is specified as well as a surface charge density η_j. Γ is approximated by the plane triangle Λ (normal $\boldsymbol{n}_\Lambda$).

When generating grid nodes, the first thing to do is mark on interfaces the multiregion points, wedge points, and corner points. The interfaces are then discretized by introducing other grid nodes. The basic type of interface element generated by doing this is the curved triangular element Γ which reproduces the actual surface almost exactly (Fig. 3). For the numerical process we also use the plane triangular element Λ formed by the same grid nodes as the associated element Γ. The electrically homogeneous subdomains are then filled with tetrahedrons that make up the volume elements $V^{(i)}$.

We can now discretize the VSIE formulation (12) for the E-field at reference points $k = 1, \cdots, N_k$

$$\boldsymbol{E}^{(k)} = \boldsymbol{E}^{(k)}_{\text{inc}} + \sum_{i=1}^{N_\Gamma} \Delta \boldsymbol{E}_{\text{scat}}(\Gamma^{(i)} \Rightarrow P^{(k)}) + \sum_{i=1}^{N_V} \Delta \boldsymbol{E}_{\text{scat}}(V^{(i)} \Rightarrow P^{(k)}) \quad (13)$$

where N_k is the number of reference points, N_Γ the number of interface elements, and N_V the number of volume elements. The symbol $\Rightarrow$ is used to indicate the integral contribution of Γ or V to a reference point P.

As the scatter contributions $\Delta \boldsymbol{E}_{\text{scat}}$ show linear dependence on the values of $\boldsymbol{E}^{(k)}$, we are provided with a linear system of N_k equations. The associated matrix is full (see [18]).

2) Classification of Interface Elements: In order to partially compensate for this numerical disadvantage we use sorting methods when calculating the convolution integral in (12) or the scatter contribution in (13). To this end, the interface elements are classified with respect to their distance from the reference grid node Q.

a) Adjoining interface elements (Fig. 4): In order to calculate the scatter contributions to Q we must perform an analytical integration over curved elements Γ which takes into account details of the local geometry and surface charge distribution (see Section II-C). Simple numerical integration methods such as the Gaussian quadrature are not accurate enough.

b) Interface elements in close proximity: The elements that lie within close proximity to Q are defined as those whose separation from Q is not more than six times the mean element dimension. For these elements it is enough to perform numerical seven-point integration over plane elements Λ with an additional solid angle correction for the normal contribution (similar to the calculations described in Section II-C for adjoining elements).

c) Distant elements: For more distant elements, a one-point integration in applied.

3) Nodal Normal Definitions: The electrical interfaces are represented by plane/curved triangles Λ/Γ. For many practical applications these interfaces can be assumed to be smooth, i.e., the surface normal (and curvature) depends continuously on position. This continuity no longer exists when a curved smooth interface at Q is reproduced using plane triangular elements $\Lambda^{(i)}$ $(i = 1, \cdots, N)$ meeting at Q. In this case, the direction of element normals $\boldsymbol{n}^{(i)}_\Lambda$ near Q changes abruptly. In contrast, if we use an arrangement of curved triangles $\Gamma^{(i)}$ $(i = 1, \cdots, N)$ associated with $\Lambda^{(i)}$ for the reproduction of this interface, we can define a common node normal $\boldsymbol{n}$ at Q for all cases of $\Gamma^{(i)}$ $(i = 1, \cdots, N)$ that adjoin grid node Q ($\boldsymbol{n}$ can be generated by suitably weighting the surface normals $\boldsymbol{n}^{(i)}_\Lambda$, $i = 1, \cdots, N$, see below and [23]). Because all $\Gamma^{(i)}$ $(i = 1, \cdots, N)$ show the same normal $\boldsymbol{n}^{(i)} = \boldsymbol{n}$ at Q, the continuity of the interface normals at the grid node Q is implicitly guaranteed.

If Q represents a corner, wedge, or multiregion point, then the interfaces are assumed to be smooth in sections. The interface corner points (such as Q in Fig. 4), wedge points, and multiregion points are treated using the same numerical procedure, which can be described as follows.

Let us assume that M smooth interface sections meet at multiregion point Q (for example, at every corner point of a cube meet $M = 3$ smooth interface sections; at every point on a cube's edge, $M = 2$ smooth interface sections meet). Each interface section $m = 1, \cdots, M$ can be made up of N_m (curved) triangles that meet at Q. This way, we can generate for each interface section m one node normal $\boldsymbol{n}_m$ $(m = 1, \cdots, M)$ in the immediate vicinity of Q. A tangential plane is defined perpendicular to each node normal $\boldsymbol{n}_m$ (see Fig. 6). Following [23], the node normals $\boldsymbol{n}_m$ are defined using weighted mean values of the surface normals $\boldsymbol{n}^{(i)}_\Lambda$. Mean value generation is only done using the triangles that go to make up surface section m at Q

$$\boldsymbol{n}_m = \frac{\sum_{i=1}^{N_m} |\Lambda^{(i)}| \cdot \boldsymbol{n}^{(i)}_\Lambda}{\left| \sum_{i=1}^{N_m} |\Lambda^{(i)}| \cdot \boldsymbol{n}^{(i)}_\Lambda \right|}, \qquad m = 1, \cdots, M \quad (14)$$

where $|\Lambda^{(i)}|$ is the area of the triangle $\Lambda^{(i)}$, N_m is the number of interface elements making up a surface section m at Q. This definition covers the case of the smooth surface at Q mentioned at the beginning ($M = 1$, $N_1 = N$).

4) Quasi-Static Approximations: To calculate the scatter field contribution from $\Gamma^{(i)}$ to a reference point $P(r)$ in the immediate vicinity [in accordance with (13)], we can perform a quasi-static approximation $(k|\boldsymbol{r} - \boldsymbol{r}'| \ll 1)$ in (6). This

gives, from (2)

$$\Delta \boldsymbol{E}_{\text{scat}}(\Gamma^{(i)} \Rightarrow P(\boldsymbol{r})) \cong \frac{1}{4\pi\epsilon_b}\int_{\Gamma^{(i)}} \eta(\boldsymbol{r}') \cdot \frac{\boldsymbol{r}-\boldsymbol{r}'}{|\boldsymbol{r}-\boldsymbol{r}'|^3}\, d^2r' \qquad i = 1, \cdots, N. \quad (15)$$

This is the basic equation for the analytical integration using the interface elements (see Section II-C).

C. Integration over Adjoining Interface Elements

For the general case, we assume N curved triangular elements $\Gamma^{(i)}$ $(i = 1, \cdots, N)$ of the type shown in Fig. 3, which meet at a node Q (shown schematically in Fig. 4). Note that the numerical methods outlined below are valid for smooth boundaries as well as for corners, wedges, and multiregion points. For Q we define a δ-spherical neighborhood $V_\delta(Q)$ with a local radius of δ. This $V_\delta(Q)$-sphere cuts a circular segment $\Gamma_\delta^{(i)}$ out of every adjoining interface element $\Gamma^{(i)}$. The selected value of δ is small enough in relation to the size of $\Gamma^{(i)}$ to allow us to assume that $\Gamma_\delta^{(i)}$ is a small plane triangular interface element with the surface local normal $\boldsymbol{n}^{(i)}$ and the local surface charge density value $\eta^{(i)}$ [see (11) and (14)]. This implicitly gives δ information on the curvature of the discretized surface, and allows us to estimate δ from the dimensions of the adjoining elements (see Appendix). The $\Gamma_\delta^{(i)}$s are used to calculate the singular scatter contributions in $V_\delta(Q)$. In ideal conditions the numerically determined results should be independent of the specific choice of $\delta(Q)$. If the surfaces are smooth enough, this actually happens, as shown in Section II-C-4. To every $\Gamma_\delta^{(k)}$ $(k = 1, \cdots, N)$ adjoining the grid node Q, a reference point $P^{(k)}$ is given by shifting Q an infinitesimally small distance along the line bisecting the contact angle of $\Gamma_\delta^{(k)}$ (Fig. 5). The relation $\|P^{(k)} - Q\| \ll \delta$ holds with respect to the local radius δ. Further splitting of $P^{(k)}$ along the local normal $\boldsymbol{n}^{(k)}$ yields $P_{+/-}^{(k)}$ where this shift is characterised by $\|P^{(k)} - P_{+/-}^{(k)}\| \ll \|P^{(k)} - Q\|$. Each surface charge element $\Gamma^{(i)}$ contributes a scattered E-field to $P_{+/-}^{(k)}$ according to (15). Following [24], this contribution is separated into a normal component $\Delta \boldsymbol{E}_{\text{norm}}^{(i)}$ (parallel to $\boldsymbol{n}^{(i)}$) and a tangential component $\Delta \boldsymbol{E}_{tg}^{(i)}$. Thus, (15) becomes

$$\begin{aligned}\Delta \boldsymbol{E}_{\text{scat}}(\Gamma^{(i)} \Rightarrow P_{\pm}^{(k)}) &= \Delta \boldsymbol{E}_{\text{norm}}(\Gamma^{(i)} \Rightarrow P_{\pm}^{(k)}) + \Delta \boldsymbol{E}_{tg}(\Gamma^{(i)} \Rightarrow P_{\pm}^{(k)}) \\ & k = 1, \cdots, N;\ i = 1, \cdots, N. \end{aligned} \quad (16)$$

The normal scatter contribution consists of a *local term*, which depends on geometric details of $\Gamma_\delta^{(i)}$ in relation to $P_{+/-}^{(k)}$, and a *global term*, which reflects the complement $\Gamma_{>\delta}^{(i)}$. The latter term is sensitive specifically to the curvature of the surface element $\Gamma^{(i)}$. However, it is independent of the particular (differential) shift of $P_{+/-}^{(k)}$, and therefore $P_{+/-}^{(k)}$ can be substituted by Q.

Now let us outline numerical calculation of normal contributions of $\Gamma^{(i)}$ to the scattered E-field at $P_{+/-}^{(k)}$.

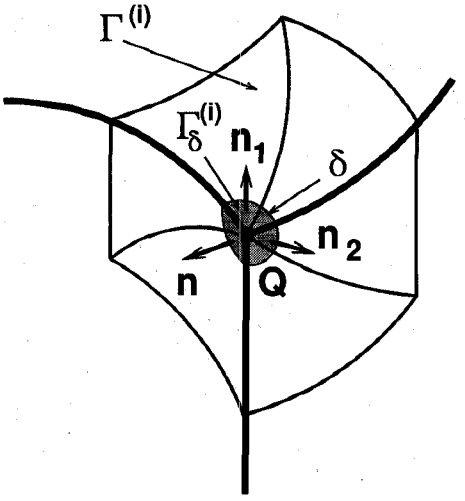

Fig. 4. Elements adjoining grid node Q. Node normal definitions. An interface corner point (comparable with a cube vertex) is the meeting place of three smooth curved interface sections. The sections are separated from each other by interface edges (thick lines). In this case, each section is made discrete using two curved triangles Γ, giving Q six adjoining elements. We cannot define for Q a unique surface normal. However, for each interface section we can define a node normal in the direct vicinity of Q, giving Q a total of three nodal normals. The direction of a node normal to a particular interface section is equivalent to the average of the normals to the plane triangular elements Λ (not shown here, see Fig. 3) that represent that section (in this case two triangles).

1) Normal Local Contribution: The relationship between a surface element $d^2\boldsymbol{r}'$ with normal $\boldsymbol{n}$ at $\boldsymbol{r}'$ and the solid angle (visual angle) subtended by $d^2\boldsymbol{r}'$ at $\boldsymbol{r}$ is given by (see [25])

$$\frac{\{\boldsymbol{n}(\boldsymbol{r}') \cdot (\boldsymbol{r}-\boldsymbol{r}')\} \cdot d^2r'}{|\boldsymbol{r}-\boldsymbol{r}'|^3} = -d\Omega(\boldsymbol{r}, \boldsymbol{r}', \boldsymbol{n}). \qquad i = 1, \cdots, N. \quad (17)$$

Since $\Gamma_\delta^{(i)}$ are assumed to be plane, $\boldsymbol{n}(\boldsymbol{r}')$ is constant for every $\Gamma_\delta^{(i)}$. Thus, setting $n(\boldsymbol{r}') = \boldsymbol{n}^{(i)}$ $(i = 1, \cdots, N)$ in (17) and subtituting (17) into (15) or (16) the normal contribution of each $\Gamma_\delta^{(i)}$ to $P_{+/-}^{(k)}$ is given by

$$\Delta \boldsymbol{E}_{\text{norm}}(\Gamma_\delta^{(i)} \Rightarrow P_{\pm}^{(k)}) = \frac{1}{4\pi\epsilon_b} \boldsymbol{n}^{(i)} \eta^{(i)} \Omega^{(k,i)} \operatorname{sign}(\boldsymbol{n}^{(i)} \cdot (\boldsymbol{r}-\boldsymbol{r}')) \quad (18)$$

$$i = 1, \cdots, N,\ k = 1, \cdots, N, \qquad \text{where} \quad 0 \le \Omega^{(k,i)} \le 2\pi.$$

Fig. 5 shows that $\Omega^{(k,i)}$ is delimited by the vector $Q - P^{(k)}$ and the tangential vectors of the edges of $\Gamma_\delta^{(i)}$ at Q. Particularly important is that $\Omega^{(k,i)}$ is independent of δ. For $\boldsymbol{r} \to \boldsymbol{r}'$ (i.e., $i = k$) we obtain $\Omega^{(k,k)} = 2\pi$. In this case

$$\Delta \boldsymbol{E}_{\text{norm}}(\Gamma_\delta^{(k)} \Rightarrow P_{\pm}^{(k)}) = \pm \frac{1}{2\epsilon_b} \boldsymbol{n}^{(k)} \eta^{(k)} \qquad k = 1, \cdots, N \quad (19)$$

which is identical to the normal "self-contribution" of a charged interface and yields the correct jump of the normal E-field on the interface (see also [18]). The "special case" of a smooth interface around a grid node is given naturally by (18), because in this case all $\boldsymbol{n}^{(i)}$ $(i = 1, \cdots, N)$ are identical and therefore $\Omega^{(k,i)} = 0$ for all $i \neq k$.

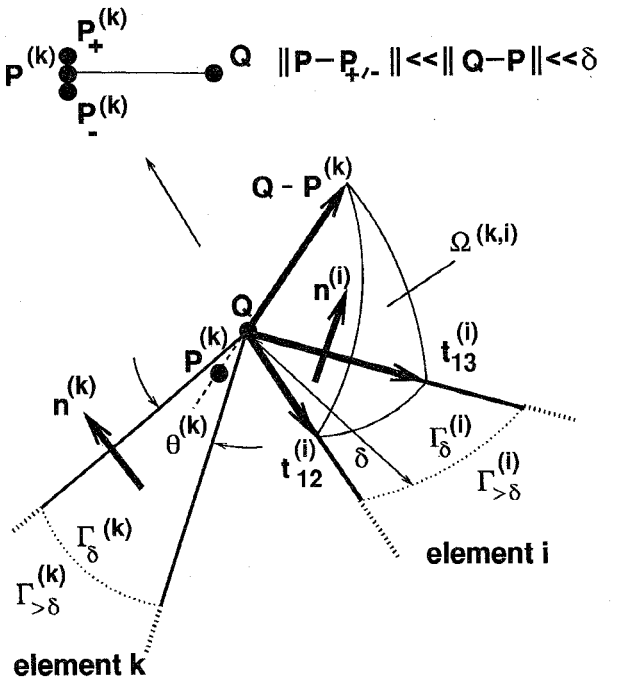

Fig. 5. Q's neighborhood. Splitting of grid node Q to process the local normal scatter field contributions. The reference point $P^{(k)}$ is given by shifting Q an infinitesimally small distance along the line bisecting the contact angle of $\Gamma_\delta^{(k)}$. Further splitting of $P^{(k)}$ along the local normal $\boldsymbol{n}^{(k)}$ yields the pair of reference points for field determination $P_{+/-}^{(k)}$. At every $P^{(k)}$ a local charge density $\eta^{(k)}$ as well as local normal $\boldsymbol{n}^{(k)}$ is specified. While the local normal self-contribution of the element $\Gamma^{(k)}$ to $P_{+/-}^{(k)}$ is proportional to the solid angle $\Omega^{(k,k)}$, $\Omega^{(k,k)} = 2\pi$ (here not shown), the local normal contribution of the contacting surface charge element $\Gamma^{(i)}$ is proportional to the solid angle $\Omega^{(k,i)}$ and is equal for both points $P_{+/-}^{(k)}$. $\Omega^{(k,i)}$ is delimited by the vector Q-$P^{(k)}$ and the tangential vectors of the edges of $\Gamma_\delta^{(i)}$ at Q ($\boldsymbol{t}_{12}^{(i)}$ and $\boldsymbol{t}_{13}^{(i)}$).

2) Normal Global Contribution: The normal contribution of the curved surface element $\Gamma_{>\delta}^{(i)}$ is calculated again on the basis of (15). This contribution is zero for noncurved triangles. Since $\delta \gg \|Q - P^{(k)}\|$, the scatter contribution is independent of the particular location of $P_{+/-}^{(k)}$. According to Fig. 6, the solid (visual) angle of $\Gamma_{>\delta}^{(i)}$ as seen from Q_1, $\Omega(Q_1, \Gamma^{(i)})$, ($Q_1$ is identical with Q) is formed in good approximation by Q_1Q_2, Q_1Q_3, Q_1Q_2', Q_1Q_3' ($Q_{2/3}'$ are the projections of $Q_{2/3}$ on the tangential plane of $\Gamma^{(i)}$ at Q_1 (perpendicular to $\boldsymbol{n}_1^{(i)} \equiv \boldsymbol{n}^{(i)}$ on $\Gamma_\delta^{(i)}$ at Q_1). As another approximation, the solid angle $\Omega(Q_1, \Gamma^{(i)})$ can be separated from the integral and the contributions from $\eta_j^{(i)}$ ($j = 1, \cdots, 3$) can be weighted according to the curvature (given by the angles β, see Fig. 6). Finally we get

$$\Delta \boldsymbol{E}_{\text{norm}}(\Gamma_{>\delta}^{(i)} \Rightarrow Q_1) \approx \frac{1}{4\pi\epsilon_b} \cdot \boldsymbol{n}_1^{(i)} \cdot \Omega(Q_1, \Gamma^{(i)}) \sum_{j=1}^{3} \eta_j^{(i)} \cdot w_j^{(i)} \quad i = 1, \cdots, N \tag{20}$$

$$w_1^{(i)} = \frac{1}{3}$$

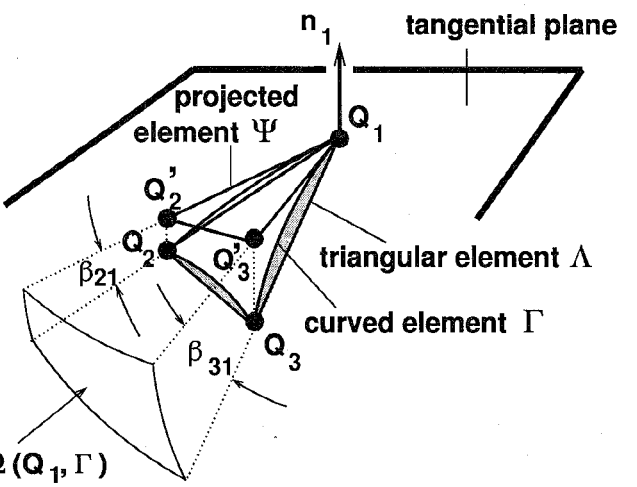

Fig. 6. Projecting the curved triangular interface element Γ onto the tangential plane defined by the node normal in the immediate vicinity of Q_1 (see Figs. 3 and 4). The projected triangle is called Ψ. The curvature-dependent, global normal scatter field contribution (direction $\boldsymbol{n}_1$) made by the surface $\Gamma_{>\delta}$ at Q_1 is proportional to the solid angle $\Omega(Q_1, \Gamma)$ subtended by $\Gamma_{>\delta}$ at Q_1. A good approximation of this solid angle is given by the triangular sides Q_1Q_2, Q_1Q_3, Q_1Q_2', Q_1Q_3'. When calculating the tangential scatter field contributions (perpendicular to $\boldsymbol{n}_1$), a good approximation of Γ can be achieved by replacing it with the projection Ψ (assuming that the curvature is not too large).

$$w_2^{(i)} = \frac{2\beta_{21}^{(i)}}{3(\beta_{21}^{(i)} + \beta_{31}^{(i)})}$$

$$w_3^{(i)} = \frac{2\beta_{31}^{(i)}}{3(\beta_{21}^{(i)} + \beta_{31}^{(i)})}.$$

Clearly, the more curved part of $\Gamma_{>\delta}^{(i)}$ gives a larger contribution to the normal component. For noncurved interface elements ($\Gamma \equiv \Lambda \equiv \Psi$ in Fig. 6) the solid angle $\Omega(Q_1, \Gamma^{(i)})$ is zero and consequently the global normal contribution disappears.

The *tangential component* proves to be nearly independent of the curvature of the interface around Q_1, provided the solid angles $\Omega(Q_1, \Gamma^{(i)})$ ($i = 1, \cdots, N$) are not extremely large, i.e., the used grid is not too coarse. Therefore, the projection of $\Gamma^{(i)}$ into the tangential plane $\Psi^{(i)}$ (defined by the normal $\boldsymbol{n}_1^{(i)} \equiv \boldsymbol{n}^{(i)}$) is employed for numerical calculation (Fig. 6). No dependence on the specific location of $P_{+/-}^{(k)}$ is seen.

Using Cartesian coordinates in the triangle $\Psi^{(i)}$ according to Fig. 7 the integral of (15) reduces to

$$\Delta \boldsymbol{E}_{tg}(\Psi^{(i)} \Rightarrow Q) = -\frac{1}{4\pi\epsilon_b} \int_{\Psi^{(i)}} \eta(x, y) \cdot \frac{x\boldsymbol{x}^0 + y\boldsymbol{y}^0}{(x^2 + y^2)^{3/2}}\, dx\, dy \quad i = 1, \cdots, N. \tag{21}$$

The tangential scatter contribution is predominantly influenced by the spatial variation of the charge density distribution, which is approximately given by linear interpolation

$$\eta(x, y) = ax + by + \eta_1. \tag{22}$$

Insertion of (22) into (21) yields, first, a nonsingular part from $ax + by$, which reflects the variation of $\eta(x, y)$ relative to η_1 and is therefore called here the gradient term.

Second, a singular integral emerges from the constant η_1, which is therefore called here the singular term. Mainly the near-range part of Ψ around Q affects this integral.

A description of the numerical calculation of both parts of $\Delta \boldsymbol{E}_{tg}$ is given below.

3) Tangential Gradient Term: The integration over $\Psi^{(i)}$ with reference to (15) is performed using local Cartesian coordinates as shown in Fig. 7 defining the line over Q_1Q_2' as abscissa (again $Q_1 \equiv Q$). We have shown the results for the case $\theta_{1/2}^{(i)} \leq \pi/2$ which is typically fulfilled for most of the triangles in a 3-D tetrahedral grid. In the case of $\theta_{1/2}^{(i)} > \pi/2$, formulas are slightly different (see [26]).

Integrals of (21) are analytical and after some algebra we obtain

$$\Delta \boldsymbol{E}_{tg}^{(\mathrm{grad})}(\Psi^{(i)} \Rightarrow Q_1) = -\frac{1}{4\pi\epsilon_b}\sum_{j=2}^{3}(\eta_j^{(i)} - \eta_1^{(i)}) \cdot \{(\alpha_{j1}^{(i)})_x \cdot \boldsymbol{x}^0 + (\alpha_{j1}^{(i)})_y \cdot \boldsymbol{y}^0\} \qquad i = 1, \cdots, N \quad (23)$$

where

$$(\alpha_{21}^{(i)})_x = -H + \frac{(h+H)x_3}{ax_2} - (1 - g - f_I)\frac{h_2}{b} - (1 - g + f_I)\frac{H}{b} \quad (23a)$$

$$(\alpha_{21}^{(i)})_y = \frac{y_3 + Hx_3}{cx_2} - (1 - g - H_2 f_{II})\frac{1}{q} + \left(-H + \frac{x_3}{cx_2} - Hh_2 \cdot f_{II}\right)\frac{H_2}{q} \quad (23b)$$

$$(\alpha_{31}^{(i)})_x = -\frac{H}{a} + \frac{x_2}{y_3} - \left(\frac{x_2}{y_3} - c + \frac{x_2}{y_3} \cdot h_2^2 \cdot f_I\right)\frac{1}{b} \quad (23c)$$

$$(\alpha_{31}^{(i)})_y = -\frac{H}{c} + \left(\frac{x_2}{y_3} - c + \frac{x_2}{y_3} \cdot h_2 \cdot f_{II}\right)\frac{H_2}{q} \quad (23d)$$

with the gradients $h = y_3/x_3$, $h_2 = y_3/(x_2 - x_3)$ as well as $H = 1/h$, $H_2 = 1/h_2$ the geometrical factors: $a = (1 + h_2)^{1/2}$, $b = 1 + h_2^2$, $c = (1 + H_2)^{1/2}$, $q = 1 + H_2^2$, $p = (x_3^2 + y_3^2)^{1/2}$, $g = (x_3^2 x_2^{-2} + y_3^2 x_2^{-2})^{1/2}$ and with logarithmic functions

$$f_I = \frac{\ln(x_2\sqrt{b} + x_2) - \ln(p\sqrt{b} + x_3 - y_3h_2)}{\sqrt{b}}$$

$$f_{II} = \frac{\ln(p\sqrt{q} + y_3 - x_3H_2) - \ln(x_2\sqrt{q} + x_2H_2)}{\sqrt{q}}.$$

The solution is independent of δ.

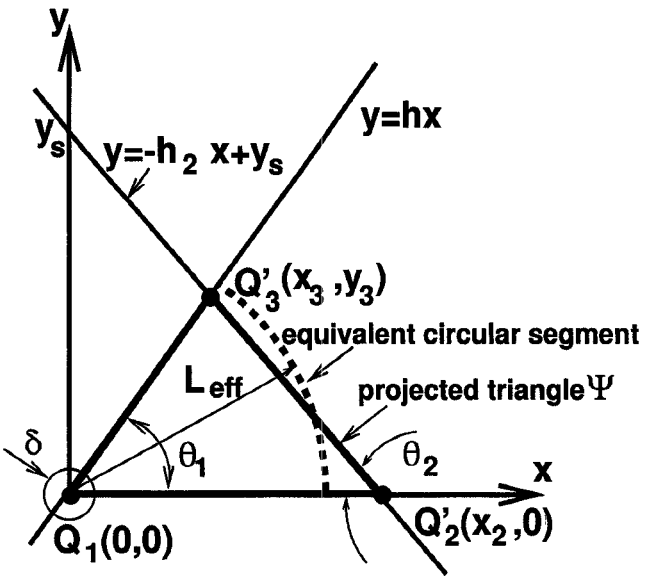

Fig. 7. Definition of the local coordinates (x, y) used for calculating the tangential scatter field contributions made by a projected triangular interface element Ψ. In order to avoid sign-dependence when integrating in Cartesian coordinates, the axes x, y perpendicular to $\boldsymbol{n}_1$ are selected so that the triangle Ψ lies within the positive region of x and y (always possible for interior angles $\theta_1 \leq \pi/2$). The x axis runs along the side Q_1Q_2'. The gradient term is calculated in cartesian coordinates x, y; the calculation of the singular term is performed using polar coordinates ρ, φ for an equivalent circular segment with the same interior angle and area as Ψ (radius L_{eff}).

4) Tangential Singular Term: For calculating the second integral (inserting the constant η_1 into (21)), local polar coordinates ρ, φ with respect to Q_1 are introduced yielding

$$\Delta \boldsymbol{E}_{tg}^{(\mathrm{sing})}(\Psi^{(i)} \Rightarrow Q_1) \approx -\frac{1}{4\pi\epsilon_b}\int_{(\rho=0)}^{L_{\mathrm{eff}}^{(i)}}\int_{(\varphi=0)}^{\theta_1^{(i)}} \eta(x, y) \cdot \frac{\boldsymbol{x}^0\cos\varphi + \boldsymbol{y}^0\sin\varphi}{\rho}\, d\varphi\, d\rho \qquad i = 1, \cdots, N. \quad (24)$$

Here, the projected triangle $\Psi^{(i)}$ has been replaced by a disc segment of apex angle θ_1 and radius L_{eff} with the same area as the original element $\Psi^{(i)}$ (compare Fig. 7)

$$L_{\mathrm{eff}}^{(i)} = \sqrt{\frac{2|\Psi^{(i)}|}{\theta_1^{(i)}}} = \sqrt{\frac{x_2^{(i)}y_3^{(i)}}{\theta_1^{(i)}}}.$$

For calculating (24), a small disc with radius $\rho = \delta_{\mathrm{av}}$ is omitted around the point Q_1. Solving the integral in (24) we obtain

$$\Delta \boldsymbol{E}_{tg}^{(\mathrm{sing})}(\Psi^{(i)} \Rightarrow Q_1) \approx -\frac{\eta_1^{(i)}}{4\pi\epsilon_b}\{(\alpha_{11}^{(i)})_x \cdot \boldsymbol{x}^0 + (\alpha_{11}^{(i)})_y \cdot \boldsymbol{y}^0\} \qquad i = 1, \cdots, N \quad (25)$$

where

$$(\alpha_{11}^{(i)})_x = \sin(\theta_1^{(i)}) \cdot \ln\left(\frac{L_{\mathrm{eff}}^{(i)}}{\delta_{\mathrm{av}}}\right) \quad (25a)$$

$$(\alpha_{11}^{(i)})_y = \{1 - \cos(\theta_1^{(i)})\} \ln\left(\frac{L_{\text{eff}}^{(i)}}{\delta_{\text{av}}}\right). \qquad (25b)$$

For a smooth interface at point Q_1, i.e., $(\theta^{(1)}+, \cdots, +\theta^{(i)}+, \cdots, +\theta^{(N)} = 2\pi)$, the sum of the tangential contributions (25a) and (25b) originating from the points in the disc is zero if we integrate all the triangles adjoining point Q_1. Thus, the singular term is independent of the value of δ_{av}. If the interface at point Q_1 is not smooth, the integral contributions will remain dependent on the exclusion radius δ_{av}. Our reasons for selecting δ_{av} are explained in detail in the Appendix.

III. Discussion and Conclusion

We have presented an efficient algorithm using the VSIE method for 3-D field calculation in electrically inhomogeneous media which performs explicit E-field calculation (i.e., not by using the H-field or potential) directly on any electrical interface combination. The code is working on the basis of nonuniform nodal linear tetrahedral elements and is capable of calculating arbitrary inhomogeneous patient models.

In global field calculation methods (IE, BEM), one of which is the VSIE method, the open radiation conditions are satisfied in the formulation using the Green's function of the background medium. Unlike most local methods (FEM, FDTD, FIT), only the actual domain of interest must be discretized and not the surrounding background medium. However, there is the numerical disadvantage that, because of the global behavior of Green's function, the method leads to full linear equation systems.

The VSIE method is particularly precise in dealing with electromagnetic fields near the numerically critical multiregion points without overestimating the E-field singularities present there. By splitting the integral equation into a volume and a surface term (VSIE-formulation) we can calculate the field discontinuities at the places they actually occur, i.e., directly on the interfaces. To do this we "split" grid nodes on the interface and treat them as pairs of reference points, allowing us to explicitly calculate the field on both sides of the interface. The field values at the two reference points nevertheless remain related due to the shared value for polarization surface charge density. The performance of the limes $\boldsymbol{r} \rightarrow \boldsymbol{r}'$ ("self-contribution") of the strongly singular surface integral using polarization surface charge density allows us to join together the inhomogeneous regions while satisfying all boundary conditions (see also [18]). The field contributions are split into physically distinct tangential and normal contributions in order to take into account the specific local interface geometry. In order to avoid overestimating the influence of the singularity, an optimal grid-dependent omission radius is estimated for linear interpolations using local polarization charge shifts. The plausibility of the estimate has been confirmed using energy studies (see Appendix).

In the VSIE method, a numerical procedure (such as Gaussian quadrature) is not suitable for elements bordering on one reference point for surface integration. Instead, analytical solutions are locally applied that describe the field behavior more accurately than numerical methods (even if the local analytical solutions are of a partially approximative nature (quasi-static approximation, disregard of curvature in tangential contributions, etc.) and only allow linear field interpolation). The reason for this lies in the strongly singular behavior of the Green's function gradient. This behavior causes numerical integration (in which the surface is approximated by a group of integration points) to be extremely sensitive with regard to the geometrical location and number of integration points on the element. Geometrical details such as interface curvature and position of interface triangles in relation to multiregion points play a particularly important part in determining the correct field values on the interfaces (and near the interfaces). Scatter contributions can be described using suitably defined solid angles. Here too, it would be very time-consuming to numerically calculate the field near the interfaces with a similar accuracy to that achieved using these analytical expressions.

Appendix
Estimation of the Average Exclusion Radius δ for Linear Nodal Elements

The singular term for the tangential direction in (25) is dependent on δ. For a smooth interface at grid node Q, the sum of the tangential contributions (25a) and (25b) originating from the points in the disc is zero if we integrate all the triangles adjoining point Q_1. Thus, the singular term is independent of the value of δ_{av}. If the interface at point Q_1 is not smooth (multiregion points, points on interface corners and interface wedges), the integral contributions will remain dependent on the exclusion radius δ_{av}.

It is therefore important to understand the implications of the choice of δ. For $\delta \rightarrow 0$, the tangential scatter contribution of each element $\Gamma^{(i)}$ at the reference point would be infinite. This singularity is caused by the "infinitely sharp edge" of the abruptly ending surface charge density on $\Gamma^{(i)}$. In order to approximate this singular field behavior by using the linear interpolations of surface charge density we assume a "roundness" or "fuzziness" of corners and edges which is dependent on the problem in hand and whose extent is given by δ. The value of δ must be chosen in relation to the size/extent of the elements; if it is too small it will lead to exaggeration of the singularity (corner, wedge, multiregion point), and if too large it will give rise to unjustifiable inaccuracy in the consideration of interfaces (see the numerical energy study below).

The singularity at Q_1 can be "naturally" resolved as shown in Fig. 8 by modifying the linearly interpolated surface charge density $\eta \rightarrow \overline{\eta}$ by defining $\overline{\eta}_1^{(i)} = 0$. The charge at Q_1 resulting from $\eta_1^{(i)}$ is apportioned in equal amounts $Q'_{2/3}$ and shifted away from Q_1, guaranteeing the conservation of charge

$$\int_{\Psi^{(i)}} \eta(\boldsymbol{r}')\, d^2r' = \int_{\Psi^{(i)}} \overline{\eta}(\boldsymbol{r}')\, d^2r' \qquad i = 1, \cdots, N \qquad (26)$$

on $\Psi^{(i)}$. Thus: $\overline{\eta}_{2/3}^{(i)} = \eta_{2/3}^{(i)} + \eta_1^{(i)}/2$.

Now we assume that the tangential contribution (21) to Q_1 from $\eta^{(i)}(\boldsymbol{r}')$ with omission $\delta^{(i)}$ should be equal to the

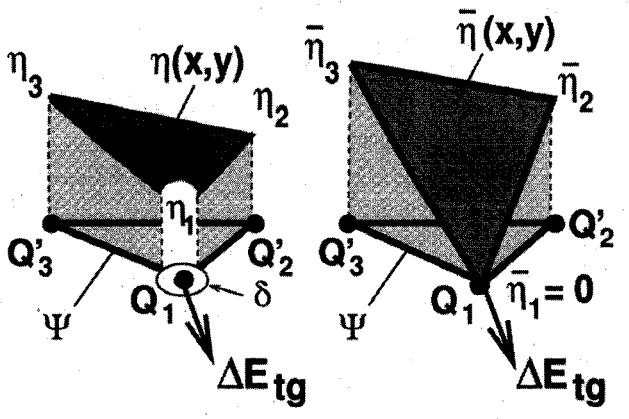

Fig. 8. An estimate of the optimum exclusion radius δ for calculating the singular tangential contributions on the projected triangle. The singularity at Q_1 is resolved by modifying the surface charge density $\eta \rightarrow \overline{\eta}$, if $\overline{\eta}_1$ is defined as 0. In order to guarantee conservation of charge, the charge at Q_1 resulting from η_1 is split equally between $Q'_{2/3}$ and shifted away from Q_1. This produces $\overline{\eta}_{2/3} = \eta_{2/3} + \eta_1/2$. We can find a value of δ due to the assumption that the tangential contribution to Q_1 from $\eta(\boldsymbol{r}')$ with omission δ (left) should be equal to the tangential contribution from $\overline{\eta}(\boldsymbol{r}')$ to Q_1 (right).

tangential contribution from $\overline{\eta}^{(i)}(\boldsymbol{r}')$ to Q_1 (see Fig. 8)

$$\int_{\delta^{(i)}}^{L_{\text{eff}}^{(i)}} \eta(\boldsymbol{r}')\vec{\nabla}' g(Q_1, \boldsymbol{r}')\, d^2r' \equiv \int_0^{L_{\text{eff}}^{(i)}} \overline{\eta}(\boldsymbol{r}')\vec{\nabla}' g(Q_1, \boldsymbol{r}')\, d^2r' \qquad i = 1, \cdots, N. \quad (27)$$

Equating the coefficients of η_1 on both sides gives [see (21) and (22)]

$$(\alpha_{11}^{(i)})_{x/y}\Big|_{\delta^{(i)}} - (\alpha_{21}^{(i)})_{x/y} - (\alpha_{31}^{(i)})_{x/y} \equiv \frac{1}{2} \cdot ((\alpha_{21}^{(i)})_{x/y} + (\alpha_{31}^{(i)})_{x/y}) \qquad i = 1, \cdots, N. \quad (28)$$

With (23a)–(23d) and (25a) and (25b) we obtain the following approximation

$$(\alpha_{21}^{(i)})_{x/y} + (\alpha_{31}^{(i)})_{x/y} \cong \frac{(\alpha_{11}^{(i)})_{x/y}\Big|_{\delta^{(i)}}}{\ln\left(\frac{L_{\text{eff}}^{(i)}}{\delta^{(i)}}\right)} \qquad i = 1, \cdots, N. \quad (29)$$

From (28) and (29) we gain (independent of the coordinates x, y)

$$\alpha_{11}^{(i)}\Big|_{\delta^{(i)}} = \frac{1.5\alpha_{11}^{(i)}\Big|_{\delta^{(i)}}}{\ln\left(\frac{L_{\text{eff}}^{(i)}}{\delta^{(i)}}\right)} \qquad i = 1, \cdots, N. \quad (30)$$

Therefore, independent of the surface charge

$$\delta^{(i)} = e^{-1.5} \cdot L_{\text{eff}}^{(i)} \qquad i = 1, \cdots, N.$$

(In the 2-D TE-case, analogously, the quotient of the optimal "exclusion radius" and of the line element length proves to be e^{-2}.)

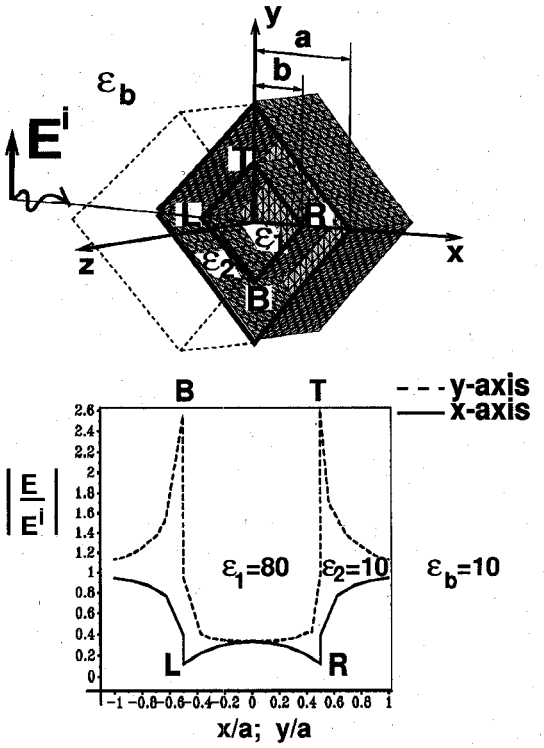

Fig. 9. Arrangement for calculating the E-field inside a two-layered cube. Outside edge = 1.4142 a, inside edge = 1.4142 b, $b = a/2$ (2a, 2b: diagonals in plane of symmetry $z = 0$). View of symmetry plane $z = 0$: the illustration shows half of the interface elements in the fine tetrahedral grid (24 576 tetrahedra). The cube is surrounded by a background medium (dielectric constant ϵ_b, wave propagation constant k). The incident plane wave is polarised in the y direction and is propagating in the x direction. The diagram on the bottom shows the E-field distribution for $q = 1$, i.e., $\delta = \delta_{\text{av}}$ (see Fig. 10) along the x and y axis of the cube. The field maxima in the plane $z = 0$ form at the poles T and B of the "inner" cube (medium electric contrast: $\epsilon_1/\epsilon_0 = 80$; $\epsilon_2/\epsilon_0 = \epsilon_b/\epsilon_0 = 10$). The field minima appear at the side points R and L. The VSIE results correspond qualitatively to theoretically predicted field behavior from [2]: compare maxima at T/B with Fig. 2(c) in [2], compare minima at R/L with Fig. 2(g) in [2].

Averaging using all $i = 1, \cdots, N$ interface elements $\Gamma^{(i)}$ at Q_1 gives us an expression for the average exclusion radius δ_{av}

$$\delta_{\text{av}} = \frac{e^{-1.5}}{N} \cdot \sum_{j=1}^{N} L_{\text{eff}}^{(i)}. \quad (31)$$

In the following, the selection $\delta = \delta_{\text{av}}$ will be also made plausible by varying δ and simultaneously considering the stored energy and, as additional test, E-field distribution in the problem domain V (Figs. 9–11).

The problem domain V is given by a layered dielectric cube. Assume a propagation of plane wave parallel to the diagonal across the plane of symmetry $z = 0$, as shown in Fig. 9. The origin is the center of the cube, and points R, L, T, B are specified. The layered cube is discretized using tetrahedral grids (coarse and fine grid containing 3 072 and 24 576 tetrahedra, respectively, see also Fig. 9). The field behavior on the cube's plane of symmetry at $z = 0$ may be expected to correspond to the field behavior around an infinitely long square dielectric cylinder running parallel to z (2-D TE case). This represents an analogy with test cases in [2], where the E-field at a 2-D-TE interface wedge is analytically calculated as a superposition of solutions for an electric and

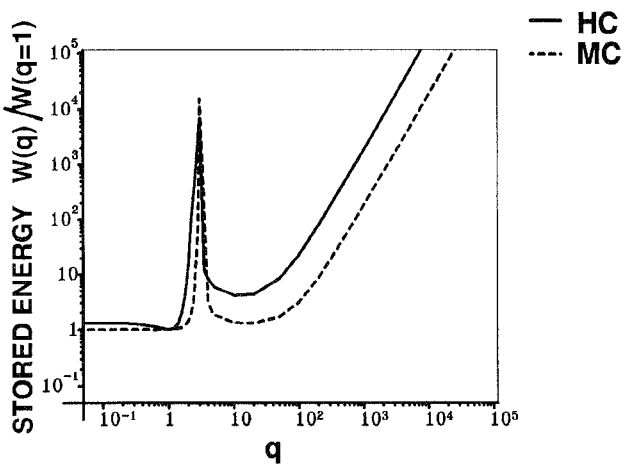

Fig. 10. Energy studies for optimum determination of the omission radius δ for calculation of the tangential scatter contributions of triangular interface elements. The diagram shows the relative stored energy $W(q)/W(q=1)$ in a layered cube for high ($\epsilon_1/\epsilon_2 = 78/1$, HC curve) and medium ($\epsilon_1/\epsilon_2 = 80/10$, MC curve) electrical contrasts in relation to the variation parameter $q = q(\delta) = \ln(L_{\text{eff}}/\delta)/\ln(L_{\text{eff}}/\delta_{\text{av}})$. δ_{av} is the optimum value of δ previously theoretically estimated ($q = 1$ for $\delta = \delta_{\text{av}}$). The graph shows that the stored energy is at a minimum in the range $0 < q < 2$ This range is studied in more detail in Fig. 11.

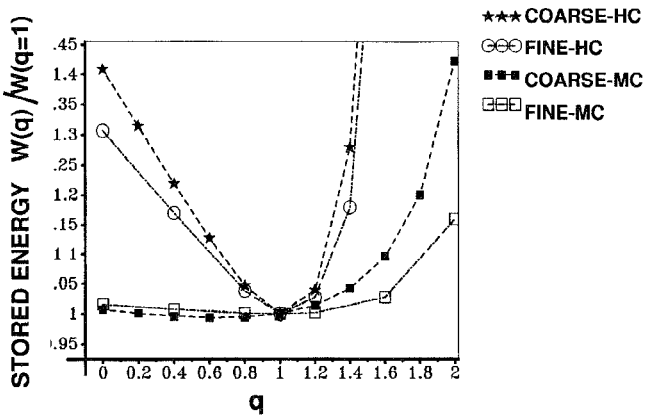

Fig. 11. A comparison between energy values $W(q)/W(q=1)$ for a coarse (3 072 tetrahedra) and fine (24 576 tetrahedra) cube grid, and for high (HC) and medium (MC) electrical contrast in the range $0 < q < 2$. The energy minimum is in fact located at/near the value $q = 1$, which has been previously theoretically estimated, even if deviations arise when determining the energy minimum because of numerical inaccuracies in integration (field singularities at corners and wedges), particularly with the coarse grids. The minimum is heavily accentuated when the contrast is high. Using a finer grid localizes the influence of δ variations on the field distribution (the global energy curves become flatter).

a magnetic wall. The local nature of the wedge singularities in question means that the dimensions of these structures are small in relation to the incident wavelength. If we study the VSIE integrals (12) we find that for larger wavelengths the contribution from the surface integral is dominant. Thus, we can perform our energy studies with good approximation for the quasi-static limes case ($kb \ll 1$, $ka \ll 1$ in Fig. 9) assuming that the investigated structures are surrounded by an infinitely large background medium (dielectric constant ϵ_b). Furthermore, we assume that the cube's outer layer has the same electrical material properties as the background medium ($\epsilon_2 \equiv \epsilon_b$ in Fig. 9). The variation studies are performed for two combinations ϵ_1/ϵ_2. The dielectric constants are selected according to the material properties at 90 MHz, assuming zero conductivity to avoid energy losses and to allow a qualitative comparison of the E-field distribution with cases presented in [2]. The first combination ϵ_1/ϵ_2 simulates the water/air boundary with a very high electrical contrast ($\epsilon_1/\epsilon_0 = 78$, $\epsilon_2/\epsilon_0 = 1$, i.e., $\epsilon_1/\epsilon_2 = 78$, abbreviation HC); the second simulates the muscle/fat boundary with a medium electrical contrast ($\epsilon_1/\epsilon_0 = 80$, $\epsilon_2/\epsilon_0 = 10$, i.e., $\epsilon_1/\epsilon_2 = 8$, abbreviation MC). The abscissas in Fig. 10–11 are labeled with the variation parameter q, $q = q(\delta) = \ln(L_{\text{eff}}/\delta)\ln(L_{\text{eff}}/\delta_{\text{av}})$ ($q = 1$ for $\delta = \delta_{\text{av}}$). Only the physically practicable values of q are considered ($q > 0$, i.e., $\delta < L_{\text{eff}}$).

A. Variation Study of Stored Energy and Qualitative E-Field Comparison

The correct solution in a dielectric problem domain V should simultaneously show a minimum in stored electric energy

$$W = \frac{1}{2}\int_V \epsilon |\boldsymbol{E}|^2 \, dV. \tag{3}$$

Varying δ we can observe (Figs. 10 and 11), that a minimum in stored energy in fact occurs at $q = 1$ (i.e., for $\delta = \delta_{\text{av}}$) as theoretically estimated above, even if deviations arise when determining the energy minimum because of numerical inaccuracies in integration (field singularities at corners and wedges), particularly with the coarse grids. As expected, the influence of variations in δ decreases (or becomes more locally limited) as the grid becomes finer, resulting in the minimum becoming flatter (Fig. 11).

As additional test, the actual field distribution can be qualitatively investigated (e.g., field behavior at wedge points R, L, B, and T).

An analysis of the qualitative field distribution restricts the range to $0 < q < 2.2$, which in fact includes the value $q = 1$ for the optimum omission radius theoretically found above. Only in this range of q do the physically correct minima and maxima appear at the wedge points (see the field distribution for $q = 1$ in Fig. 9: field minima at R and L correspond qualitatively to Fig. 2(c) in [2]; field maxima at B and T, correspond qualitatively to Fig. 2(g) in [2]). In the range $2.2 < q < 3.5$, i.e., when δ is reduced further, stored energy values increase (as shown in Fig. 10). In this range the calculated field distribution shows maxima at all four wedge points, which is strongly different from [2] (field distributions for $q \neq 1$ are not shown in this paper). True, further reduction of δ ($3.5 < q < 100$) leads to a reduction in energy, but the field distribution shows minima at all four wedge points, which does not correspond to [2] neither. For $q > 100$, i.e., $\delta/L_{\text{eff}} \to 0$, the field strength at all wedge points tends towards zero, and at the grid points neighboring the wedge points huge maxima occur that increase as δ tends towards zero giving the increasing values of stored energy. We can therefore conclude that if δ is too small, incorrect results will be obtained by the code.

This model study gives qualitative information about the influence of variations in δ on a physical parameter which

should be minimal. Keeping in mind that deviations may arise when determining the energy minimum because of numerical inaccuracies in integration (field singularities at corners and wedges), particularly with the coarse grids, we can certainly specify a narrow range around the value of $q = 1$, which is the value theoretically found above.

ACKNOWLEDGMENT

The authors would like to thank Prof. G. Mönich and to Prof. W. John, Technische Universität Berlin, Institut für Hochfrequenztechnik, for valuable discussions on scattering in inhomogeneous media.

REFERENCES

[1] J. Meixner, "The behavior of electromagnetic fields at edges," *IEEE Trans. Antennas Propagat.*, vol. AP-20, pp. 598–602, 1972.
[2] J. B. Andersen and V. V. Solodukhov, "Field behavior near a dielectric wedge," *IEEE Trans. Antennas Propagat.*, vol. AP-26, pp. 598–602, 1978.
[3] K. D. Paulsen, "Finite, boundary, and hybrid method solution of the Maxwell equations for simulating hyperthermia treatment of cancer," Ph.D. dissertation, Dartmouth College, Hanover, NH, 1986.
[4] W. Delbare and D. de Zutter, "Space-domain Green's function approach to the capacitance calculation of multiconductor lines in multilayered dielectrics with improved surface charge modeling," *IEEE Trans. Microwave Theory Tech.*, vol. 37, pp. 1562–1568, 1989.
[5] G. Mur, "The finite-element modeling of three-dimensional electromagnetic fields using edge and nodal elements," *IEEE Trans. Antennas Propagat.*, vol. 41, pp. 948–953, 1993.
[6] W. E. Boyse and A. A. Seidl, "A hybrid finite element method for 3-D scattering using nodal and edge elements," *IEEE Trans. Antennas Propagat.*, vol. 42, pp. 1436–1442, 1994.
[7] K. D. Paulsen, X. Jia, and J. M. Sullivan, Jr., "Finite element computations of specific absorption rates in anatomically conforming full-body models for hyperthermia treatment analysis," *IEEE Trans. Biomed. Eng.*, vol. 40, pp. 933–945, 1993.
[8] A. P. M. Zwamborn and P. M. van den Berg, "The three-dimensional weak form of the conjugate gradient FFT method for solving scattering problems," *IEEE Trans. Microwave Theory Tech.*, vol. 40, pp. 1757–1766, 1992.
[9] N. Kuster, "Multiple multipole method for simulating EM problems involving biological bodies," *IEEE Trans. Biomed. Eng.*, vol. 40, pp. 611–620, 1993.
[10] D. M. Sullivan, O. P. Gandhi, and A. Taflove, "Use of the finite-difference time-domain method for calculating EM absorption in man models," *IEEE Trans. Biomed. Eng.*, vol. 35, pp. 179–185, 1988.
[11] D. M. Sullivan, "A frequency-dependent FDTD method for biological applications," *IEEE Trans. Microwave Theory Tech.*, vol. 40, pp. 532–539, 1992.
[12] T. G. Jurgens and A. Taflove, "Three-dimensional contour FDTD modeling of scattering from single and multiple bodies," *IEEE Trans. Antennas Propagat.*, vol. 41, pp. 1703–1708, 1993.
[13] J. Toftgard, S. N. Hornsleth, and J. B. Andersen, "Effects on portable antennas of the presence of a person," *IEEE Trans. Antennas Propagat.*, vol. 41, pp. 739–746, 1993.
[14] J. De Moerloose and D. De Zutter, "Surface integral representation radiation boundary condition for the FDTD Method," *IEEE Trans. Antennas Propagat.*, vol. 41, pp. 890–896, 1993.
[15] R. Pontalti *et al.*, "The frequency dependent FDTD method for multi-frequency results in microwave hyperthermia treatment simulation," *Phys. Med. Biol.*, vol. 38, pp. 1283–1298, 1993.
[16] T. Weiland, "On the numerical solution of Maxwell's equations in the field of accelerator physics," *Particle Accelerators*, vol. 15, pp. 245–292, 1984.
[17] T. Weiland, "Die Diskretisierung der Maxwell-Gleichungen," *Phys. Bl.*, vol. 42, pp. 191–201, 1986.
[18] P. Wust, J. Nadobny, M. Seebass, J. M. Dohlus, W. John, and R. Felix, "3-D Computation of E-fields by the volume-surface integral equation (VSIE) method in comparison with the finite-integration theory (FIT) method," *IEEE Trans. Biomed. Eng.*, vol. 40, pp. 745–759, 1993.
[19] Y. Saad and M. H. Schultz, "GMRES: A generalized minimal residual algorithm for solving nonsymmetric linear systems," *SIAM J. Sci. Statist. Comput.*, vol. 7, pp. 856–869, 1986.
[20] J. Nadobny, P. Wust, P. Deuflhard, G. Mönich, and R. Felix, "Examination of the singular field behavior at arbitrary interfaces in biological media using the volume-surface integral equation method," *IEEE Trans. Biomed. Eng.*, submitted for publication, 1996.
[21] C. Müller, *Foundations of the Mathematical Theory of Electromagnetic Waves*. New York: Springer-Verlag, 1969.
[22] M. Seebass, "3-D-Computersimulation der interstitiellen Mikrowellen-Hyperthermie von Hirntumoren," Bericht Nr. CVR 1/90, Institut für Radiologie und Pathophysiologie, Deutsches Krebsforschungszentrum, Heidelberg, 1990.
[23] X. Yuan, D. R. Lynch, and K. D. Paulsen, "Importance of normal field continuity in inhomogeneous scattering problems," *IEEE Trans. Microwave Theory Tech.*, vol. 39, pp. 638–642, 1991.
[24] O. D. Kellogg, *Foundations of Potential Theory*. New York, Dover, 1929.
[25] J. D. Jackson, *Classical Electrodynamics*, 2nd ed. New York: Wiley, 1975.
[26] J. Nadobny, "Berechnung und Optimierung elektromagnetischer Felder im Patienten bei regionalen Hyperthermieanwendungen," Ph.D. dissertation, Technische Universität Berlin, Institut für Hochfrequenztechnik, 1992.

Jacek Nadobny was born in 1959 in Kalisz, Poland. He received the M.S. degree in electrical engineering from the Technical University Berlin, Germany, in 1987, and received the Ph.D. degree in the Department of Electrical Engineering at the Technical University Berlin in 1993.

He is presently a Research Engineer in the Strahlenklinik and Poliklinik, Virchow-Kliniku, Humboldt University, Berlin, and in the Konrad Zuse Zentrum, Berlin, where he is engaged in the development of computer simulation for hyperthermia cancer therapy and applicator design.

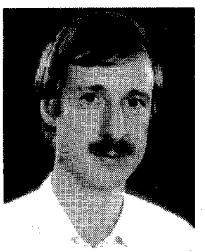

Peter Wust was born in Berlin, Germany, in 1953. He received the M.S. degree in physics (Dipl-Phys.) in 1978 and the M.D. degree (Dr. Med.) in 1983 from the Free University of Berlin.

Since 1984 he has worked with the Radiological Department of the University Hospital of Berlin (Virchow-Klinikum, Humboldt University). He achieved the board certification of Radiation Oncology in 1990, and is working as Assistant Professor for Radiation Oncology since 1993. He has done research work on nuclear physics (heavy ions), medical physics, and radiation oncology. Since 1988 he has been working in methodical and clinical aspects of hyperthermia in cancer therapy, and is coordinator of a special research project on hyperthermia.

Martin Seebass was born in 1960 in Bad Neuenahr, Germany. He received the diploma degree in physics from the University of Bonn in 1983 and the Ph.D. degree in physics from the University of Heidelberg in 1990.

From 1985 to 1991 he worked at the German Cancer Research Center in Heidelberg. Since May 1991 he has been with the Konrad Zuse Zentrum, Berlin, where he is involved with the development of computer simulation for hyperthermia cancer therapy.

Peter Deuflhard, was born near Munich, Germany, in 1944. He received the physics diploma degree at the Munich Institute of Technology in 1968 and the Ph.D. degree in mathematics from the University of Cologne in 1972.

He is presently Director of the internationally renowned Konrad-Zuse-Zentrum in Berlin and full Professor of Scientific Computing at the Free University of Berlin. From 1978 to 1986 he was full Professor of Mathematics (with specialty in Numerical Analysis) at the University of Heidelberg and moved to Berlin thereafter to build the Konrad-Zuse-Zentrum as a center of High Performance Scientific Computing. His special fields of interest are differential equation modeling, efficient simulation and optimization. He has worked in many different application areas including space technology, chemical engineering, medicine, and electronics. His main research contributions are algorithms for the fast and reliable solution of ordinary and partial differential equation systems, typically large scale and originating from engineering or medicine.

Roland Felix was born in Berlin, Germany, May 15, 1938. He received the M.D. degree in 1962 at the University of Munich.

In 1964, he started his scientific work at Bonn University. His main interest was heart and pulmonary diseases as well as cerebral microcirculation. Since 1975, he was mainly engaged in computed tomography and contrast media development. Since 1978, he has been full Professor of Radiology at Freie Universität Berlin, Klinikum Rudolf Virchow. In 1983, together with Schering Company, he began work on the development of Gadolinium-DTPA, a new contrast agent for magnetic resonance imaging. In 1986, he set up the division of Therapeutical Hyperthermia and established telecommunication.